Journal of Physics: Conference Series **3224** (2026) 042037 doi:10.1088/1742-6596/3224/4/042037

Benchmarking aerodynamic codes for 2D aerofoils with leading edge erosion

A Meyer Forsting[1], A Dicholkar[1], NN Sørensen[1], AS Olsen[1], C Bak[1], JN Theron[2], A Aihara[3], M Caboni[4], A Koodly Ravishankara[4], K Vimalakanthan[4], D Bretos[5], B Mendez[5], G Campaña-Alonso[5,6], O Pires Jimenez[5], F Grasso[7], MS Campobasso[8] and D Maniaci[9]

[1]DTU Wind, Technical University of Denmark, Denmark; [2]Fraunhofer IWES, Germany; [3]AIST, Japan; [4]TNO, The Netherlands; [5]CENER, Spain; [6]UPM, E.T.S.I. Aeronáutica y del Espacio, Universidad Politécnica de Madrid, Spain; [7]Vestas Technology Centre Porto, Portugal; [8]School of Engineering, Lancaster University, United Kingdom; [9]Sandia National Laboratories, United States

E-mail: alrf@dtu.dk

Abstract. Increasing tip speeds and harsh environmental conditions have made leading edge erosion and roughness (LEE/LER) a major concern for the wind industry, as even mild surface damage can significantly lower aerodynamic performance and annual energy production. This paper presents an aerodynamic benchmark conducted within the framework of IEA Task 46 to assess the predictive capabilities of various CFD-RANS and viscous-inviscid interaction codes using simulations and wind tunnel measurements from the LERCat project. The benchmark focusses on the 21% thick FFA-W3-211 aerofoil across seven test cases: clean (transitional and tripped), rough (P40 and P400 sandpaper), and three 2D erosion profiles of varying severity, extracted from 3D aerofoil surfaces with realistic, high-resolution damage topographies. The study finds that while codes generally agree within the attached-flow regime in clean conditions, significant spreads occur around stall and when modelling large-scale sand roughness, where pressure drag becomes dominant. The resolved erosion cases highlight that performance is primarily driven by erosion triggering bypass transition and that it is grid dependant. Overall, the agreement between codes for predicting the performance with LEE within the aerofoil operating range is substantially better than for the clean transitional case.

1. Introduction

Increasing tip speeds combined with harsh environmental conditions have made leading edge erosion and roughness (LEE/LER) a major concern within the wind industry, as blade leading edges (LEs) have been exhibiting major damage in the form of laminate exposure or even holes after operating for only one or two years. Whilst this obviously endangers turbines structurally if left unmitigated, even mild surface roughness and erosion damage—in the order of 50 to 100 µm and thus difficult to visually detect—can significantly lower a blade's aerodynamic performance [1–4], ultimately leading to a drop in a turbine's annual energy production (AEP) [5, 6]. Establishing best practices for modelling these aerodynamic effects and identifying potential knowledge gaps is a key aim of the IEA Task 46, which brings together experts in climate, materials, and aerodynamics from both industry and academia in a joint effort to address LE

damage. A first aerodynamic benchmark assessed the predictive capabilities of different CFD-RANS and viscous-inviscid interaction codes in capturing surface roughness effects in 2D aerofoil performance polars [7], using wind tunnel measurements of the NACA 63_3-418 [5, 8] and S814 [5] profiles as reference. Even though a large variety of tools and roughness models were tested, the model spread was limited and agreed well with measurements, except around stall, where many models struggle to offer a predictive solution. Building upon the previous benchmark, here simulations are performed for the 21% thick FFA-W3-211 aerofoil [9] with roughness and erosion, corresponding to test cases performed within the Leading Edge Roughness Categorisation (LERCat) project[1]. Whilst clean, tripped and rough (sandpaper) conditions are tested as in the previous benchmark, special focus lies on simulating aerofoils with fully resolved erosion damage. For this purpose three, 2D chordwise slices with varying levels of erosion are extracted from 3D aerofoil surfaces with realistic, high-resolution damage topographies [10]. This paper compares integral and surface quantities to pinpoint differences among code predictions and uses measurements from DTU Wind's Poul la Cour wind tunnel (PLCT) as reference.

2. Benchmark cases

In total, seven test cases were defined for the FFA-W3-211 aerofoil, two clean cases (transitional, tripped/fully turbulent), two with surface roughness (P40, P400 sandpaper) and three with LEE. The clean transitional and tripped (fully turbulent) simulations provide a common baseline and, as in the first IEA Task 46 benchmark [7], participants had to incorporate the effects of roughness in their modelling efforts. The difference here was that, instead of prescribing the equivalent sand grain roughness, the participants had to estimate it independently using only the measured average sand grain size and paper thickness. This was intended to mimic the practical modelling of real-world surfaces. Our goal was to identify the degree of inter-participant variability and assess whether such subjective modelling choices lead to significant differences in predicted aerodynamic performance. The three erosion profiles extracted from the 3D surfaces created by

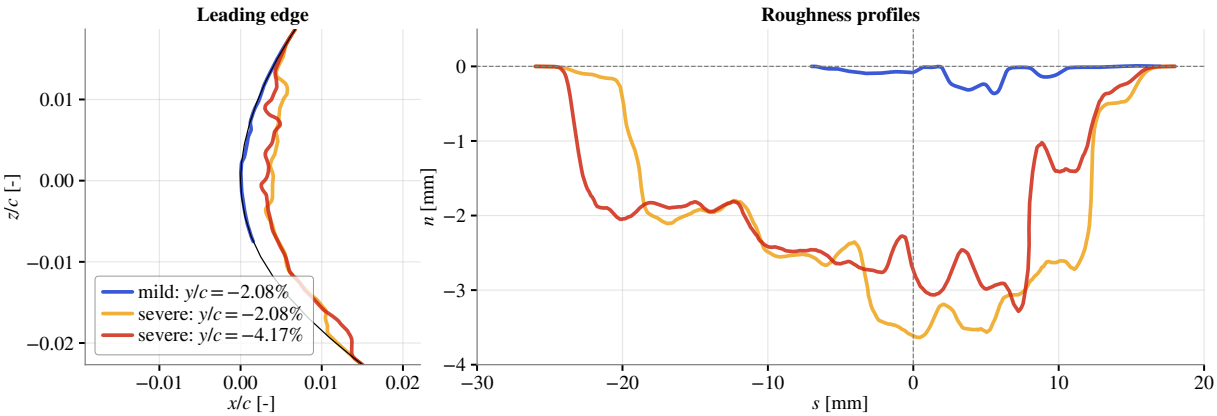

Figure 1. Benchmark cases exhibiting LEE with labels indicating the spanwise position and 3D surface from which they were extracted (refer to [10]). The LE is located at $s = 0$ and s is positive towards the suction side.

Meyer Forsting et al. [3, 10] that were to be simulated are shown in figure 1; additionally to the LE shape (left), the corresponding roughness profiles are depicted (right), with the labels

[1]Sponsored by the Danish Energy Council; Partners: DTU Wind, Vestas Wind Systems A/S, Siemens Gamesa Renewable Energy A/S, LM Wind Power A/S, Suzlon Energy Nederlands Branch, PowerCurve ApS

indicating at which spanwise position, y, and eroded surface (mild/severe) they were extracted from. The roughness profiles are provided in surface-following coordinates and reported in mm, whereas the LE profiles are normalised by the chord length, c. Whereas the mild profile serves to test the transition models [10], the two severe cases evaluate numerical robustness and separation behaviour. For a full description of the 3D roughness topographies tested and simulated within the LERCat project refer to [10]. For the clean and rough cases the participants received only the wind tunnel profile coordinates, whilst for the eroded cases the surfaces meshes from [10] were provided. These had a uniform resolution of ≈110 µm over the entire eroded region. The ambient turbulence level was given as 0.1 %—corresponding to a N factor of 8.15 [11]. This is the level attained in the PLCT [12] and generally ensures that simulated and observed transition behaviour is matched [3, 10]. Simulations had to be performed at Reynolds numbers of 3, 4.5 and 6 million for angles of attack from $-20°$ to $20°$.

3. Wind tunnel measurements

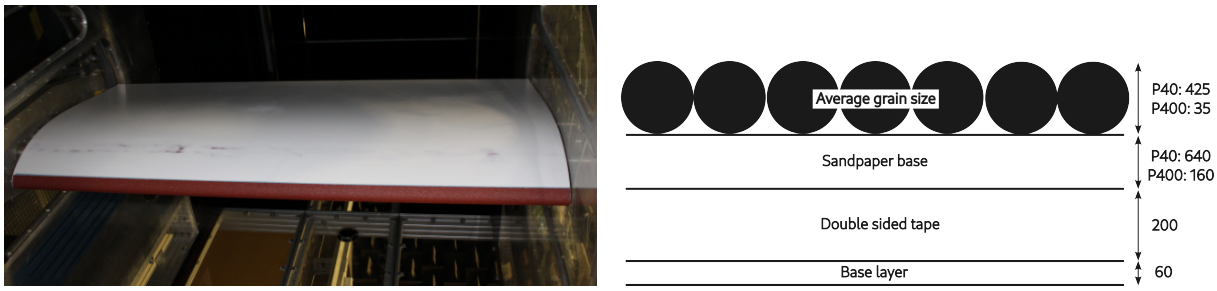

Figure 2. P40 sandpaper wrapped around the FFA-W3-211 in the PLCT (left, rotated image) and geometric definition (not to scale) of the tested P40 and P400 sandpapers (right); dimensions reported in µm.

Within the LERCat project, a painted aluminium wind tunnel model of the FFA-W3-211 [9] was tested in DTU Wind's PLCT. The model had a chord length of 900 mm and had a removable LE to allow mounting 3D prints incorporating erosion damage. An aluminium LE, which was milled together with the aft body, was used in the clean, free transition measurements. The boundary layer was tripped with zig-zag tape[2] positioned at $x/c = 0.05$ on the suction side and $x/c = 0.10$ on the pressure side. Surface roughness effects were assessed by wrapping conventional P40 and P400 sandpaper around the LE as shown in figure 2. With a width of 93 mm, it spanned from $x/c = 0.04$ on the pressure side to $x/c = 0.03$ on the suction side and was spanwise continuous. It was mounted on top of the clean aerofoil using a base layer and double-sided tape with a combined height of 260 µm. The average sandpaper grain sizes were measured to be 425 µm (P40) and 35 µm (P400) glued onto a base paper of 640 µm (P40) and 160 µm (P400) thickness, respectively. No chamfer was added towards the ends of the sandpaper to smoothen the steps. The PLCT test section is rectangular with a cross-section of 3 m × 2 m and is 9 m long. Flow enters the test section through a settling chamber equipped with a honeycomb and three turbulence-reduction screens and a 9:1 contraction. As the aerofoil model spanned the test section's entire height of 2 m, the aspect ratio was 2.2 and at maximum lift the tunnel blockage was about 8 %. The model was connected via pins to the turntables on both ends and the small gaps (<0.5 mm) between the aerofoil and section walls were sealed. A wake rake

[2] 460 µm tall including base tape, 60° opening angle and 12 mm width

positioned about two chords downstream of the trailing edge measured the total drag. In the clean configuration, lift was determined from the surface pressure distribution obtained via the aerofoil pressure taps; for all other configurations, it was derived from the wind tunnel wall pressure measurements.

4. Aerodynamic codes

Table 1. Overview of CFD solvers and simulation setups.

Org.	Solver	Turbulence	Transition	Roughness	Ambient turb.
DTU	EllipSys2D v24	k-ω SST	e^N, γ-Re_θ, γ-DLR	Knopp	✓
AIST	OF v2106	k-ω SST	γ-Re_θ	Cebeci-Bradshaw	
CENER	OF v2506	k-ω SST	γ-Re_θ	Cebeci-Bradshaw	✓
IWES	OF v2306	k-ω SST	e^N,γ-Re_θ	Cebeci-Bradshaw	
TNO	OF v2012	k-ω SST	γ-Re_θ	Dassler + Wilcox	
TNO	SU2 v8	k-ω SST/SA		Wilcox/Aupoix	

Org.: Organisation; ✓: Active

Six institutions provided submissions, using two RFOIL-based [13] approaches and three different CFD finite-volume solvers: The 2D version of the structured, multi-block code EllipSys [14], SU2 [15] and different versions of OpenFOAM (OF) [16–18]. All CFD codes solved the steady incompressible RANS equations using SIMPLE [19] or SIMPLEC [20] type algorithms and close the equations with the two-equation k-ω SST turbulence model [21], except one that used the one-equation Spalart-Allmaras (SA) [22] model. Laminar to turbulent boundary layer transition was modelled using the correlation-based γ-$Re_{\theta t}$ [23] and γ-DLR [24] models or e^N [25] type approaches. The increased friction caused by surface roughness in fully turbulent boundary layers is incorporated through the Aupoix [26] model in the SA runs and through the Knopp [27], Cebeci-Bradshaw [28] and Wilcox [29] models in the k-ω SST simulations. To also capture roughness-induced transition, TNO's OF simulations incorporated a roughness amplification A_r transport equation [4] as proposed by Dassler et al. [30]. The Wilcox model was used once the flow transitioned. No participant explicitly modelled the thickness of the sandpaper. As the γ-$Re_{\theta t}$ model responds to the local turbulence intensity some participants introduced ambient turbulence sustaining terms [31]. Additionally the EllipSys2D simulations with the γ-$Re_{\theta t}$ model employed the Kato-Launder turbulent kinetic energy production limiter [32] to avoid unphysical production within the stagnation region. Though not necessarily required with the Knopp model, rough simulations were run in conjunction with the SST viscous sublayer shielding by Hellsten-Laine [33]. AIST employs a wall function approach to set the turbulent quantities at the first off-wall cell, which allows for lower vertical resolution. SU2 runs with transition models were also submitted, but were omitted as they showed nearly no transitional behaviour and hence deemed erroneous. An overview of the numerical setups is presented in table 1, with further details regarding the CFD domains and mesh specifications available in table 2. The latter also provides the first off-wall cell height and aerofoil surface resolution for the different test cases. The clean (transitional, fully turbulent) and rough (P400, P40 sandpaper) simulations generally used the same numerical grid. Note that in the clean simulations $y^+ < 1$ required that $\Delta \lesssim 5.0\times10^{-6}$ at a Reynolds number of 3 million, dropping down to 2.5×10^{-6} at 6 million.

TNO and Vestas used the viscous-inviscid interaction solver RFOIL [13] (TNO: v3.0.4, Vestas: v2.0.1)—an extension of XFOIL [25] tailored towards wind turbine aerofoils developed by ECN, TU Delft and the NLR (Royal Netherlands Aerospace Centre)—and therefore cannot di-

Table 2. Overview of grid specifications; dimension are given in terms of chord length.

					No. of surface cells			
Org.	Topo.	Type	Domain size	$\Delta \times 10^{-6}$	TE	Clean/Rough	Mild	Severe
DTU	O	Struc.	90×90	0.5	14	512	768	960
AIST	H	Struc.	80×80	30	7	5183	5183	5182/5185
CENER	O/H*	Struc./Unstr.	$120 \times 120^{*}$	4.2	5	500	2600	2600
IWES	O	Struc.	$100 \times 100^{\star}$	2.0	14	512	768	960
TNO: OF	O	Struc.	90×90	2.0	5	700	700	700
TNO: SU2	C	Unstr.	150×150	$2.5^{\dagger}$	4	254		

Org.: Organisation; Topo.: Grid topography; Struc.: Structured; Unstr.: Unstructured; Domain size: width×height; Δ: Wall cell height; TE: Trailing edge, Mild: Mild erosion; Severe: Severe erosion
*O with 500×400 for clean/rough; ⋆300×300 for clean/rough; †0.1 for rough

rectly run the resolved erosion benchmark cases. However, TNO has implemented a roughness model [34, App. A] that allows capturing the aerodynamic effects of distributed roughness on transition, whilst Vestas uses the in-house Digital Airfoil Reconstruction Tool (DART) to correct the clean RFOIL polar data to account for the aerodynamic impact of stall, roughness and erosion. The DART corrections are based on Vestas' extensive set of wind tunnel measurements and rely on parametrising polar curves with a limited number of control points. The relative movement of those control points due to roughness/erosion from the clean reference can then be mapped onto those describing the clean RFOIL polar curves. Vestas classifies LEE within five levels and assigns aerodynamic losses according to wind tunnel measurements of aerofoils with LER and LEE [35]. Vestas' RFOIL simulations employed 197 panel nodes using a TE/LE panel density ratio of 0.15 and a panel bunching parameter of 1.0. In contrast, the TNO simulations used 160 nodes, a density ratio of 0.8, and a bunching parameter of 0.3.

5. Clean and rough test cases

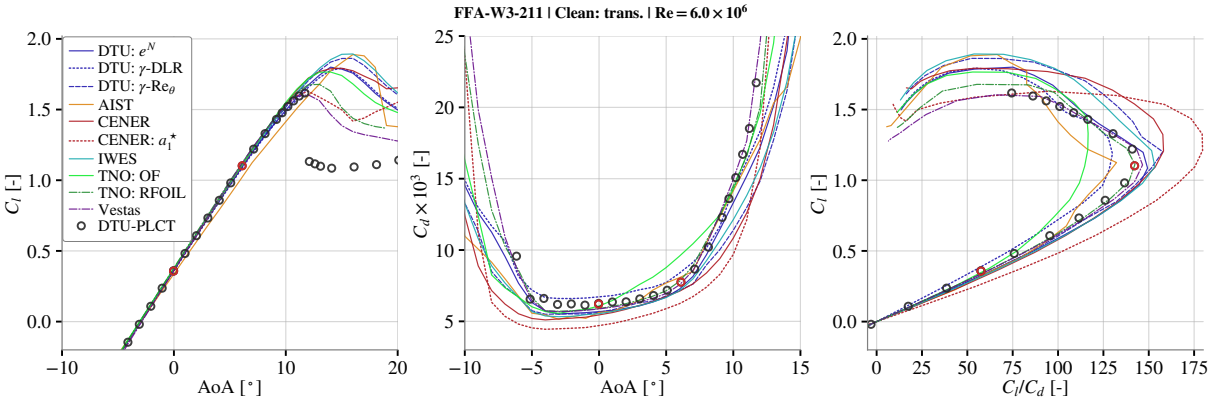

Figure 3. Performance of the clean FFA-W3-211 at a Reynolds number of 6 million, with red dots highlighting measurements at 0° and 6°.

As nowadays most outer blade sections of utility scale wind turbines operate at high Reynolds numbers (> 5 million), most results within this paper will be discussed for the highest Reynolds number only. Hence in figure 3 the clean performance predictions for the FFA-W3-211 are compared at a Reynolds number of 6 million. As shown in many previous 2D aerofoil benchmarks, lift predictions in the attached flow regime largely agree with measurements—only AIST slightly

underestimates the lift curve slope—whilst they struggle to reproduce the measured stall behaviour [36]. Indeed, the 2D RANS simulations predict stall occurring between 14°-16° with $C_{l_{\max}}$ within 1.77-1.89, whereas measurements show stall at 12° reaching substantially lower $C_{l_{\max}}$ of 1.62. Whilst none reproduce the abrupt nature and loss of lift seen in the measurements at stall, both RFOIL-based submissions agree in terms of $C_{l_{\max}}$ and stall angle. Yet RANS simulations with lowered a_1 SST model constant (CENER: $a_1^\star$)—from the default 0.31 to 0.28—reconfirm that this approach can improve stall predictions [36, 37], as it limits the overproduction of eddy viscosity within boundary layers experiencing strong adverse pressure gradients. The issue with lowering a_1 is that it alters the baseline behaviour of the SST model, lowering skin friction [37] and thereby drag, as clearly seen in the middle panel of figure 3. Ignoring the latter, though, the minimum drag lies actually within a thin band between 5.1-6.6 drag counts. However, the CFD results by TNO, CENER and AIST predict a differently shaped drag bucket, with a continuous rise in drag away from the minimum, whereas the other models and measurements show a kink around 6°, indicating a sudden forward movement of the suction side transition location. This movement is known to be delayed when using the γ-$Re_{\theta t}$ transition model [34], which ultimately leads to an overprediction of the maximum lift-to-drag ratio. The faster drag rise observed for TNO, CENER and AIST also yields lower max. C_l/C_d ratios—130 for AIST and CENER versus the 142 measured—yet they occur around the same C_l of 1.1. The RFOIL-based lift-to-drag predictions lie closest to the measurements together with the DTU simulations using the e^N transition model. The latter starts to diverge approaching stall, however, as stall is delayed as previously mentioned. The DTU results using three different transition models demonstrate how performance predictions vary with the choice of transition model. Interestingly the more recently developed γ-DLR model seems to predict the same drag bucket shape, but overestimates minimum drag, lowering the max. lift-to-drag ratio to 130.

Table 3. Selected sand grain roughness, reported as $k_s/c \times 10^{-6}$.

					TNO		
	DTU	AIST	CENER	IWES	OF*	SU2	RFOIL
P400	125	39	455	140	39	40	18
P40	1477	472	1325	1700	472	400	222

*Uses roughness height [4] and is thus reported here instead

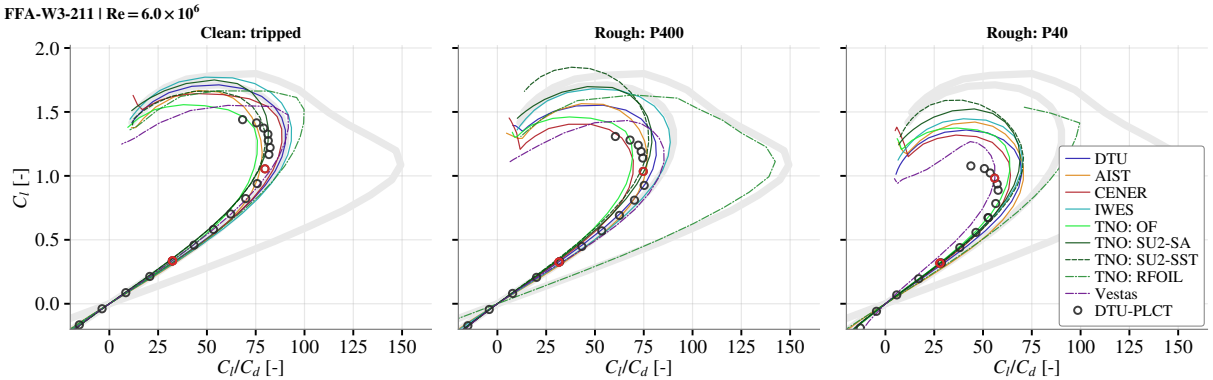

Figure 4. Performance of the FFA-W3-211 at a Reynolds number of 6 million, when tripped at the LE (left) or with P400 (middle) and P40 (right) sandpaper covering the LE. Gray lines provide clean and tripped reference (DTU).

Moving on from transitional performance, figure 4 compares predictions for the clean tripped and sandpaper cases in terms of C_l versus lift-to-drag, again at a Reynolds number of 6 million. Thick gray lines are drawn using the DTU predictions for clean transitional (with e^N) and tripped flow as visual reference. The sand grain roughness heights estimated by the participants are given in table 3; Vestas classified the P400 and P40 cases as erosion levels 1 and 4, respectively. All results show a marked drop in lift-to-drag when tripped (left)—down to 80 at 6° for the measurements—but the RFOIL-based codes show lower drag growth at higher C_l, making them attain larger lift-to-drag before stall; the latter manifests itself through strong lift-to-drag loss. Most models predict slightly larger drag than seen in the measurements, however with a height of 460 µm, the zig-zag tape used to trip the flow in the wind tunnel is likely too large, adding some unwanted pressure drag. At 6° or $C_l = 1.1$—the operating point for max. lift-to-drag in clean transitional conditions—the models lie within 74 to 89. The drop in performance from LER is captured by nearly all models in the attached regime for low (P400, middle) and extremely large roughness (P40, right) alike. However, the wind tunnel measurements show that the flow starts to separate earlier from the suction side—earlier drag growth—than predicted by any model and also stalls beforehand, especially with large roughness. This has been reported before [7] and is related to roughness models adding to friction drag only. Yet roughness also impacts pressure drag, as the flow detaches locally in the wake of individual roughness elements. The larger the elements, the greater the pressure drag. Beyond a certain size, their impact can no longer be modelled through increasing friction drag alone, thus leading to incorrect stall behaviour. Despite using different roughness models and sand grain roughness heights (see table 3), the CFD predictions at $C_l = 1.1$ lie all within 16 and 8 lift-to-drag counts for P400 and P40 sandpaper, respectively. Clearly the roughness height set in TNO's RFOIL simulations for the P400 sandpaper is not tall enough to trigger transition. This is achieved for P40, but as the additional friction from surface roughness is not accounted for, there is little difference with respect to the tripped case. The empirical correction to RFOIL by Vestas coincides with the measurements at 6°, but overestimates drag at lower angles and stalls later. When comparing to measurements it is important to note, though, that the steps towards the ends of the sandpaper are about 455 µm (P400) and 1325 µm (P40) tall. Especially the latter might have a non-negligible impact, but was not explicitly modelled by any participant. The above observations equally apply to the lower Reynolds numbers of 3 and 4.5 million for the tripped clean and rough cases. Yet, the clean transitional case clearly highlights that the correlation-based transition models (γ-$Re_{\theta t}$, γ-DLR) struggle to correctly capture Reynolds number effects. As this is not the focus of this paper refer to [24, 34, 38] for in-depth discussion on this matter.

6. Erosion test cases

Figure 5 compares the performance predicted for the FFA-W3-211 with LEE of varying severity at Reynolds numbers of 3 (top) and 6 million (bottom). Experimental results are not shown in this section, as they were conducted with spanwise varying erosion; for a discussion on 2D-3D equivalence refer to [10]. All CFD contributions explicitly resolved the erosion, but the resolution over the eroded regions varied. DTU and IWES used the provided surface mesh, which had a uniform resolution of about $120 \times 10^{-6} c$ over the erosion, whereas AIST and CENER lowered it by a factor 4 and 6, respectively. Vestas manipulated the clean polars by designating the mild case as level 1 and both severe cases as level 2 erosion. Some participants provided both, transitional and fully turbulent results. To facilitate the comparison, gray lines are again drawn for DTU's clean transitional and tripped predictions; additionally for the transitional results dots indicate angles of attack from 0° to 6° in 1° steps. The performance change with

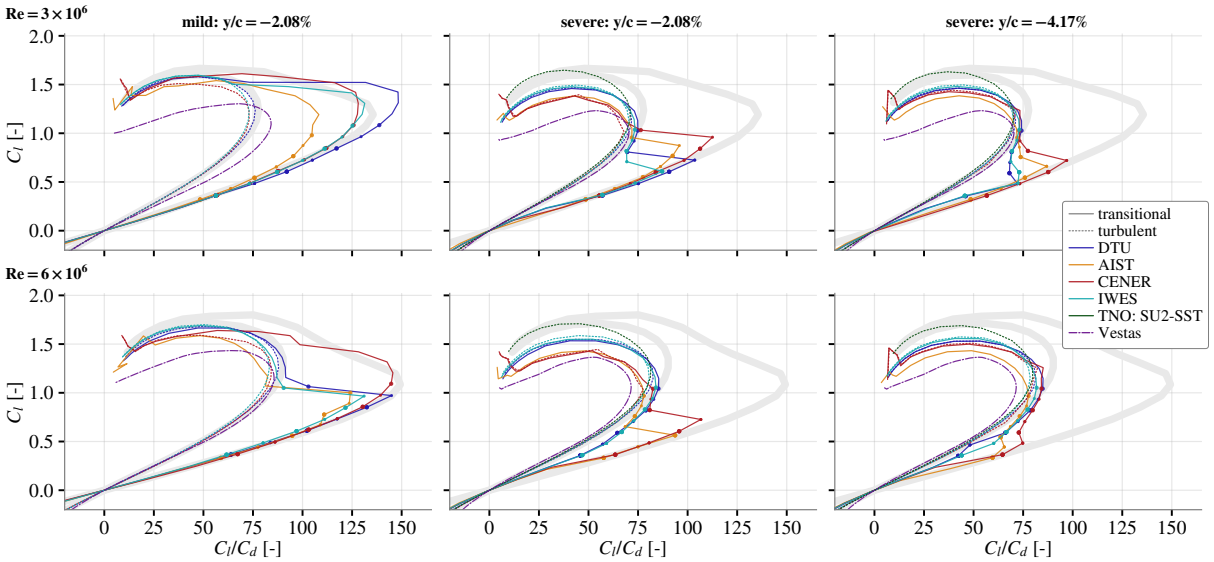

Figure 5. Performance of the FFA-W3-211 with three different erosion profiles at two Reynolds numbers. Dots indicate AoAs from 0° to 6° in 1° steps. Gray lines provide numerical predictions for clean and tripped for reference (DTU).

Reynolds number for mild erosion (left) demonstrates that, as shown by Meyer Forsting et al. [10], it influences performance by triggering transition. At a Reynolds number of 6 million all CFD models follow their respective clean transitional results before suddenly departing from them at around 6° and moving towards their tripped (turbulent) performance. At 3 million all CFD results are unchanged from the transitional ones. The criticality of the erosion in terms of triggering bypass transition, thus agrees well between the different CFD predictions. The simulations not considering transition (turbulent) all align with the clean tripped reference, indicating that there is no additional drag from mild erosion, if transition is not considered. Vestas predictions assume that the flow is tripped and hence behave accordingly. For the two slices taken from the severe erosion (middle, right) the sensitivity for erosion to trigger transition seems to be code dependent but consistent across the comparison: IWES predicts erosion impact for both slices at all Reynolds numbers, DTU only at higher Reynolds numbers, whereas AIST and CENER always exhibit some fraction of laminar flow at lower angles of attack. Yet once the flow has turned fully turbulent, which is generally the case at 6°, predictions are extremely close, varying by maximally 12 lift-to-drag counts and 0.08 in C_l. There is slightly larger variation in the prediction of $C_{l_{\max}}$, though, which also depends on the erosion geometry. All results indicate earlier stall with severe erosion which clearly differentiates it from mild erosion [10].

To further examine the differences, figure 6 compares pressure (top) and skin-friction (bottom) coefficients for CFD simulations considering transition at an angle of attack of 4° for the severe erosion slice at $y/c = -2.08\%$. Pressure and suction side are split according to the LE location and the eroded region is excluded for legibility. All codes indicate that pressure side transition is not triggered at either Reynolds number, yet as seen in the lift-to-drag polars, the AIST and CENER results also resist transition at 3 million on the suction side, unlike DTU and IWES. The CENER results only show a slow build-up in friction at 6 million, which is indicative of delayed turbulence build-up. Additionally IWES curves with lowered a_1 SST constant are shown (IWES: $a_1^\star$), which clearly demonstrates that it consistently lowers skin friction in the turbulent region of the boundary layer, thereby lowering overall friction drag as discussed earlier,

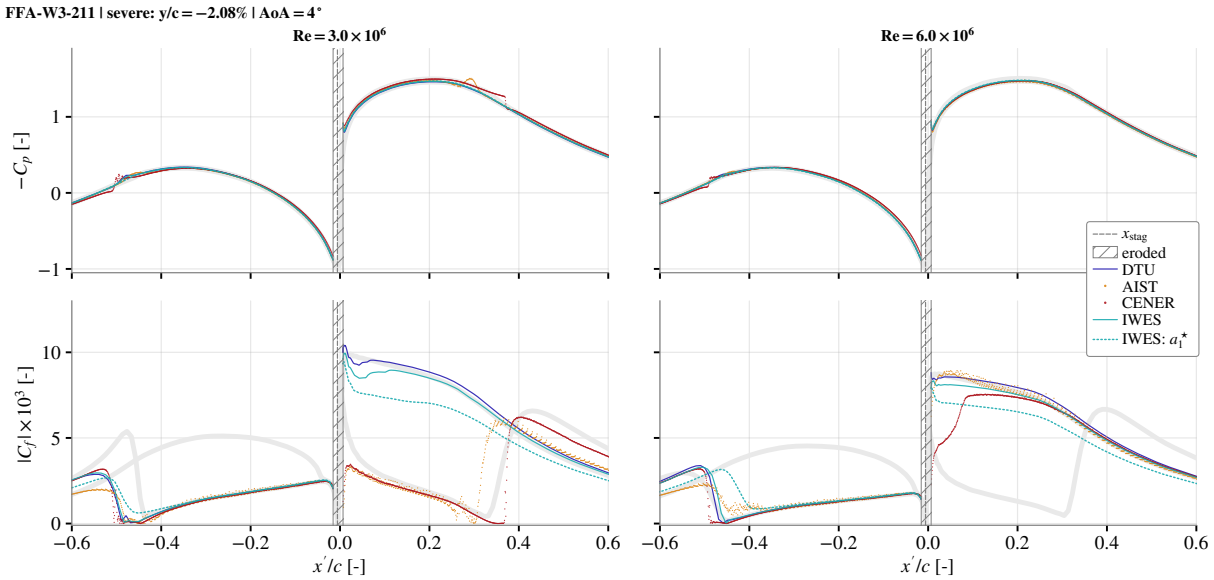

Figure 6. Pressure (top) and skin-friction (bottom) coefficients at 4° for two Reynolds numbers for the severely eroded FFA-W3-211 at $y/c = -2.08\%$; $x' < 0$ on the pressure side. Gray lines provide clean and tripped reference (DTU).

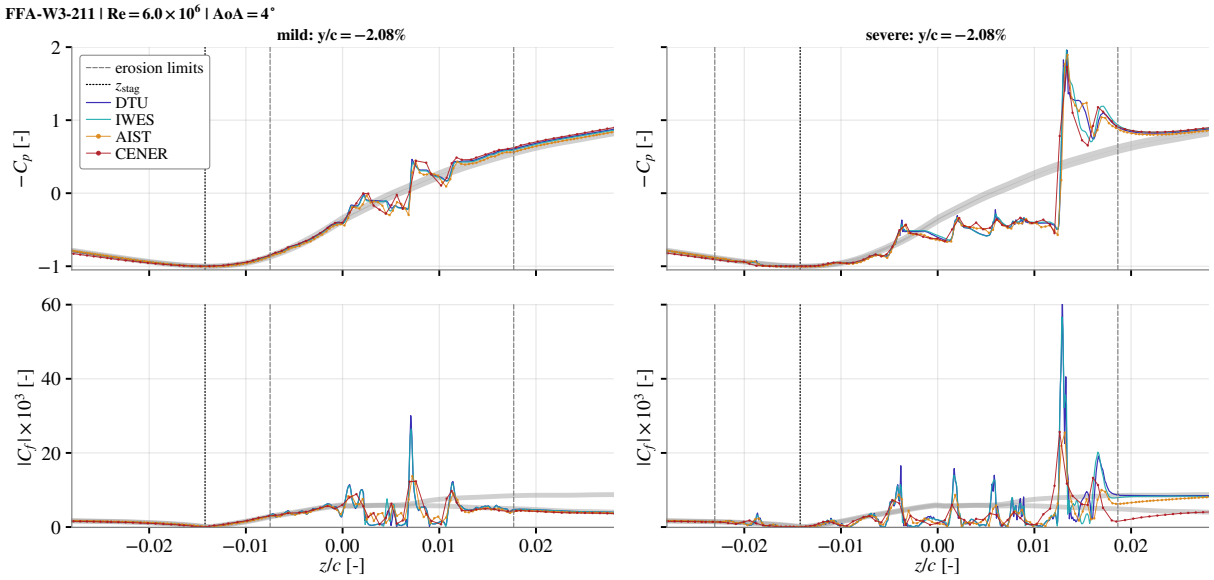

Figure 7. Pressure (top) and skin-friction (bottom) coefficients over the eroded region for mild (left) and severe (right) damage at $y/c = -2.08\%$ at 6° and 6 million. Gray lines provide clean and tripped reference (DTU).

whilst leaving pressure unchanged. Figure 7 zooms into the behaviour within the eroded zone itself by expressing pressure and skin-friction coefficient in terms of the chord-normal direction, now showing results only at 6 million, but also including results for mild erosion (left). The agreement between IWES and DTU over the mild erosion is excellent, with the curves following the transitional results outside the eroded region, as expected. The pressure variation clearly follows the erosion profile (see figure 1) with peaks in the skin-friction corresponding to areas

with strong pressure gradients and acceleration. The agreement is similarly good for the severe profile, except downstream of the pressure peak at $z/c = 0.013$; the flow seems to separate in the DTU results due to the adverse pressure gradient, whereas for IWES it does not. As both AIST and CENER used lower resolution, they do not capture peaks in the same manner, which is especially visible in the skin friction. With CENER having the lowest resolution, they also differ the most. Whether erosion triggers transition is hence closely related to the mesh resolution used to resolve it; the lower, the less likely it will trigger transition, as gradients are smoothed.

7. Conclusion

This benchmark study provides a comprehensive evaluation of state-of-the-art aerodynamic solvers in predicting the effects of leading edge damage on the FFA-W3-211 aerofoil. The comparison of CFD-RANS and viscous-inviscid interaction codes against wind tunnel measurements reveals that while lift predictions in the attached flow regime are consistent across most platforms, 2D CFD approaches continue to struggle with stall behaviour, typically overpredicting both the stall angle and maximum lift. Regarding surface roughness, existing models successfully capture performance drops for moderate cases like P400 sandpaper but struggle at extreme levels, such as P40, because they primarily account for friction drag rather than the pressure drag induced by local flow separation. For the resolved erosion cases, the main variability between predictions lay in capturing the erosion-induced onset of transition, which was identified to closely correlate with grid resolution. The lower the resolution, the later was transition triggered. As erosion severity and Reynolds number increased, differences disappeared, as erosion became a more effective transition trigger and tripped behaviour largely agreed between models.

Acknowledgements

This work was supported by the LERCat project (Danish Energy Council: EUDP-64021-2027), the AIRE project (EU: HORIZON-CL5-2021-D3-03, No. 101083716) and IEA Task 46 (Danish Energy Council: EUDP-134243-532862).

References

[1] Sareen A, Sapre C A and Selig M S 2014 Effects of leading edge erosion on wind turbine blade performance *Wind Energy* **17** 1531–1542
[2] Gaudern N 2014 A practical study of the aerodynamic impact of wind turbine blade leading edge erosion *Journal of Physics: Conference Series* **524** 012031
[3] Meyer Forsting A, Olsen A S, Sørensen N N and Bak C 2023 The impact of leading edge damage and repair on sectional aerodynamic performance *AIAA SCITECH Forum*
[4] Vimalakanthan K, van der Mijle Meijer H, Bakhmet I and Schepers G 2023 Computational fluid dynamics (CFD) modeling of actual eroded wind turbine blades *Wind Energy Science* **8** 41–69
[5] Ehrmann R S, Wilcox B, White E B and Maniaci D C 2017 Effect of surface roughness on wind turbine performance Tech. rep. Sandia National Lab.(SNL-NM), Albuquerque, NM (United States)
[6] Maniaci D, Westergaard C, Hsieh A and Paquette J 2020 Uncertainty quantification of leading edge erosion impacts on wind turbine performance *Journal of Physics: Conference Series* **1618** 052082
[7] Campobasso M S, Castorrini A, Bretos D, Mendez B, Maniaci D C, Theron J N, Meyer Forsting A, Sørensen N N, Aihara A and Vimalakanthan K 2025 Validation of the predictive capabilities of computational aerodynamics codes to assess eroded blade performance: First aerodynamic benchmark Technical report IEA Wind Task 46
[8] Pires O, Munduate X, Boorsma K, Yilmaz O C, Madsen H A and Timmer W 2018 Experimental investigation of surface roughness effects and transition on wind turbine performance *Journal of Physics: Conference Series* **1037** 052018

[9] Björck A 1990 *Coordinates and Calculations for the FFA-W1-xxx, FFA-W2-xxx and FFA-W3-xxx Series of Airfoils for Horizontal Axis Wind Turbines* (Aeronautical Research Institute of Sweden)
[10] Meyer Forsting A, Sørensen N N, Dicholkar A and Olsen A S 2025 *High-Resolution 3D CFD Simulations of Wind Turbine Aerofoils with 3D Scanned Leading Edge Roughness*
[11] Mack L M 1977 Transition and laminar instability Tech. Rep. JPL-PUBL-77-15
[12] Devenport W, Bak C, Brown K, Borgoltz A, Østerlund J and Davidsson P 2017 Design and operation of hybrid aeroacoustic wind tunnels *Von Karman Institute for Fluid Dynamics lecture series*
[13] van Rooij R A 1996 Modification of the boundary layer calculation in RFOIL for improved airfoil stall prediction Tech. Rep. IW-96087R TU Delft
[14] Sørensen N 1995 General purpose flow solver applied to flow over hills Tech. Rep. Risø-R-827(EN) RisøNational Laboratory
[15] Economon T D, Palacios F, Copeland S R, Lukaczyk T W and Alonso J J 2016 SU2: An open-source suite for multiphysics simulation and design *AIAA Journal* **54** 828–846
[16] Weller H G, Tabor G, Jasak H and Fureby C 1998 A tensorial approach to computational continuum mechanics using object-oriented techniques *Computers in Physics* **12** 620–631
[17] OpenFOAM Foundation 2024 *OpenFOAM User Guide* OpenFOAM Foundation URL `https://openfoam.org`
[18] OpenCFD Ltd 2023 *OpenFOAM Release Notes* ESI Group URL `https://www.openfoam.com`
[19] Patanker S and Spalding D 1972 A calculation procedure for heat, mass and momentum transfer in three-dimensional parabolic flows *International Journal of Heat and Mass Transfer*
[20] Van Doormaal J P and Raithby G D 1984 Enhancements of the simple method for predicting incompressible fluid flows *Numerical Heat Transfer* **7** 147–163
[21] Menter F R, Kuntz M, Langtry R *et al.* 2003 Ten years of industrial experience with the sst turbulence model *Turbulence, heat and mass transfer* **4** 625–632
[22] Spalart P and Allmaras S 1992 A One-Equation Turbulence Model for Aerodynamic Flows AIAA paper 92-0439 30th AIAA Aerospace Sciences Meeting and Exhibit, Reno, Nevada
[23] Langtry R B and Menter F R 2009 Correlation-based transition modeling for unstructured parallelized computational fluid dynamics codes *AIAA Journal* **47** 2894–2906
[24] François D G, Krumbein A, Krimmelbein N and Grabe C 2023 Simplified stability-based transition transport modeling for unstructured computational fluid dynamics *Journal of Aircraft* **60** 1773–1784
[25] Drela M and Giles M B 1987 Viscous-inviscid analysis of transonic and low reynolds number airfoils *AIAA Journal* **25** 1347–1355
[26] Aupoix B and Spalart P 2003 Extensions of the Spalart–Allmaras turbulence model to account for wall roughness *International Journal of Heat and Fluid Flow* **24** 454–462
[27] Knopp T, Eisfeld B and Bartolome Calvo J 2009 A new extension for k–ω turbulence models to account for wall roughness *International Journal of Heat and Fluid Flow* **30** 54–65
[28] Cebeci T and Bradshaw P 1977 *Momentum Transfer in Boundary Layers* (Washington, DC: Hemisphere Publishing Corporation)
[29] Wilcox D C 1988 Reassessment of the scale-determining equation for advanced turbulence models *AIAA Journal* **26** 1299–1310
[30] Dassler P, Kožulović D and Fiala A 2010 Modelling of roughness-induced transition using local variables *ECCOMAS CFD 2010* (Lisbon, Portugal)
[31] Spalart P R and Rumsey C L 2007 Effective inflow conditions for turbulence models in aerodynamic calculations *AIAA Journal* **45** 2544–2553
[32] Kato M and Launder B 1993 The modelling of turbulent flow around stationary and vibrating square cylinders paper 10-4 9th Symposium on Turbulent Shear Flows, Kyoto, Japan
[33] Hellsten A, Laine S, Hellsten A and Laine S 1997 *Extension of the k-omega-SST turbulence model for flows over rough surfaces* (AIAA) chap AIAA 1997-3577
[34] Langel C M, Chow R C, van Dam C P and Maniaci D C 2017 RANS-Based Methodology for Predicting the Influence of Leading Edge Erosion on Airfoil Performance
[35] Grasso F 2025 Leading edge erosion classification based on wind tunnel tests Presentation at the Wind Energy Science Conference (WESC) [Available Online]. Accessed: 2026-02-20
[36] Gutierrez R, Zamponi R, Ragni D, Llorente E and Aranguren P 2023 On the extension of k–ω–SST corrections to predict flow separation on thick airfoils with leading-edge roughness *Wind Energy* **26** 650–667
[37] Matyushenko A and Garbaruk A 2016 Adjustment of the k-ω sst turbulence model for prediction of airfoil characteristics near stall *Journal of Physics: Conference Series* **769** 012082
[38] Jung Y S, Vijayakumar G, Ananthan S and Baeder J 2022 Local correlation-based transition models for high-reynolds-number wind-turbine airfoils *Wind Energy Science* **7** 603–622